Fabrication of samarium strontium aluminate ceramic and deposition of thermal barrier coatings by air plasma spray process

Baskaran T [1*] and *Shashi Bhushan Arya*[1]

[1]*Department of Metallurgical and Materials Engineering, National Institute of Technology Karnataka, Surathkal, Mangaluru-575 025, India*

Abstract. Thermal barrier coatings (TBC) with the metallic NiCrAlY bond coat are often used in many aircraft engines to protect superalloy components from high-temperature corrosion thereby to improve the life of gas turbine components. The search for new TBC material has been intensified in recent years due to lack of thermo-physical properties of conventionally used Yttria stabilized Zirconia (YSZ) TBCs. Recently, the rare earth containing Samarium Strontium Aluminate (SSA) based ceramic was proposed as a new TBC material due to its matching thermo-physical properties with the substrate. The present work focused on the synthesis of SSA ceramics for TBCs application and its coatings development on Ni-based superalloy Inconel 718 substrate by air plasma spray process. The X-ray photoelectron spectroscopy (XPS) result confirmed the formation of single phase SSA ceramic after synthesis. The surface morphology of SSA TBCs is mainly composed of melted splats, semi and un-melted particles. The cross-sectional SEM micrographs did not show any spallation at the interface which indicated good mechanical interlocking between the bond coat and ceramic top coat. The Young's modulus and hardness of SSA TBCs were found to be 80 and 6.1 GPa, respectively. The load-depth curve of SSA TBC showed good elastic recovery about 47 %.

Keywords: Ceramic; Plasma spray; Superalloys; Thermal barrier coatings; Nano-indentation

1 Introduction

Thermal barrier coatings (TBC) plays an important role in providing low thermal conductivity, also act as a barrier to heat transfer between hot gas flow regions of the engine and coated superalloy substrate [1]. Presently Yttria stabilized zirconia (YSZ) has been used as a standard ceramic top coat material in TBCs applications due to its low thermal conductivity and high melting point [2]. However, due to the lack of sintering and

* Corresponding author: baskarannitk@gmail.com

phase transformation above 1200 ºC intensify the search for new ceramic top coat materials [3].

In the past decade, the new ceramics such as zirconate perovskites (SrZrO3), zirconate pyrochlores (La2Zr2O7) and several hexa aluminates materials have been proposed to replace the currently used standard material YSZ [3, 4]. Among all the new materials, the zirconate based pyrochlores exhibited low thermal conductivity, high thermal expansion coefficients and good phase stability over YSZ. However, the poor thermo-chemical compatibility with thermally grown oxide at the interface reduced the thermal cyclic life of TBC at elevated temperatures [5]. Recently, the rare earth based strontium aluminate (Ln2SrAl2O7, Ln=Sm, Gd, Nd, La, etc.) have also been proposed as a thermal barrier coating materials more particularly Sm based aluminates showed low thermal conductivity, high melting point, phase stability and higher thermal expansion coefficient at higher temperature (>1200 ºC) [6, 7]. Review of literature showed that most of the published work focused on the synthesis and thermal properties of ceramic but works on coating development and relevant studies are scarce. So, further research is required on the development of coatings of samarium strontium aluminate (Sm2SrAl2O7; SSA) ceramic for TBC applications.

In the present study, an attempt is made to synthesis the SSA ceramic in the laboratory and deposition of TBCs using air plasma spray process on nickel based super alloy substrate. The mechanical behavior of as deposited SSA ceramic, metallic bond coat and the substrate is investigated.

2 Experimental details

2.1 Synthesis of SSA powder by molten salt method

Samarium oxide (Sm_2O_3, 99.9%), Strontium carbonate ($SrCO_3$, 99.0%) and Aluminium oxide (Al_2O_3, 99.9%) were used as a starting precursor materials for the synthesis of SSA ceramic. These oxides were mixed with 0.5:0.5 eutectic compositions of potassium chloride (KCl, 99.5%) and sodium chloride (NaCl, 99.5%) for 30 min in an agate mortar. The mixture was placed in the alumina crucible and then heated up to 1100 ºC for 24 h. Final products were continuously washed with hot deionized water to remove the salts. The obtained products were further dried in the hot air oven at 120 ºC for 6 h.

2.2 Deposition of SSA ceramic by air plasma spray process

The as synthesized SSA ceramic was thermally sprayed on an Inconel 718 superalloy substrate using 55 kW F4-MB plasma gun. A metallic NiCrAlY was deposited on the substrate prior to the deposition of the ceramic top coat. The spray distance between nozzle and substrate approximately 100 mm. The feed rate of SSA ceramic powder is around 30 g/min. The thicknesses of the metallic bond coat and ceramic TBC top coat were about 50 and 100 μm respectively.

2.3 Characterization of SSA ceramic and as deposited coating

X-ray Photoelectron Spectroscopy (XPS) being used to examine stoichiometry of synthesized SSA (ESCALAB MkII, VG Scientific). Al Kα radiation (12 kV, 6 mA) was used to excite Sm 4d, Sr 3d, Al 2p, and O 1s electron from as-synthesized SSA. The obtained spectrum was calibrated with C 1s line at 285 eV.

The morphological analyses of as synthesized SSA ceramic and cross sectional studies of as deposited coatings were done using SEM (JEOL-JSM-6380LA, USA). The elemental analysis of ceramic powder and coatings were studied using Elemental Dispersive X-ray Spectroscope (EDS).

The mechanical properties such as Young's modulus, stiffness and hardness of substrate, metallic bond coat, and as deposited SSA TBCs were measured using Hysitron tribo-indenter fitted with Berkovich indenter.

3 Results and discussion

3.1 Characterization of synthesized SSA ceramic powder

A wide and high-resolution XPS spectrum of Sm, Sr, Al, and O are shown in Figs. 1 and 2 respectively. The major elements such as Sm, Sr, Al, and O were observed without any other impurities (Fig. 1). The binding energy (BE) at 284.6 eV corresponded to C 1s which is generally used as internal reference spectra (Fig. 1). The BE values at 976 eV and 1224 eV are more evident auger peaks of O and C respectively [8]. Fig. 2 (a-d) shows the high resolution XPS scan of Sm 3d, Sr 3d, Al 2p and O 1s. The Sm 3d peaks such as Sm $3d_{5/2}$ and Sm $3d_{3/2}$ were found at two distinct BE of 1084.3 eV and 1111.5 eV. The BE difference between these two peaks (27.2 eV) clearly indicated the +3 oxidation state of Sm ion (Table 1).

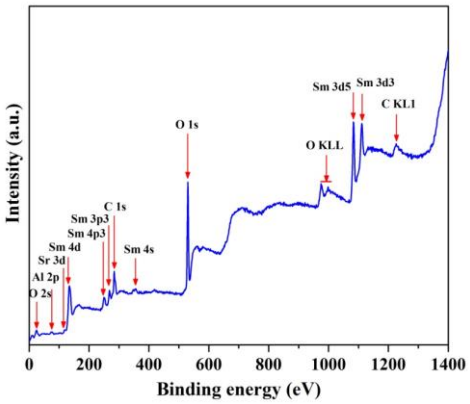

Fig. 1: XPS survey spectra of as-synthesized SSA ceramic powder.

The symmetry of Sm peak indicates that the presence of samarium ions in +3 valence state (Sm^{3+}). Two Gaussian peaks of Sr 3d peak were found at 134.06 eV and 135.8 eV corresponded to Sr $3d_{5/2}$ and Sr $3d_{3/2}$ lines, respectively in the SrO. The high resolution scan of Al (Al 2p) is shown in Fig. 2 (c) and this characteristic peak found to be at a BE of 73.03 eV. The BE values of O 1s peaks at 528.19, 529.50 and 530.10 eV revealed the presence of Al-O, Sm and /Sr-O bonds respectively. All noticed BE values of Sm_2O_3, SrO, and Al_2O_3 phases have shown good agreements with literature data's which are given in Table 1 [9-17].

Table 1: Binding energies of Sm 3d, Sr 3d, Al 2p and O 1s of synthesized SSA powder.

	Binding energy (eV)		Compound formation	
Electron level	Experimental value	Reference value	Experimentally observed	References
Sm $3d_{3/2}$	1111.5	1110.9	Sm_2O_3	(Ref 9-11)
Sm $3d_{5/2}$	1084.3	1083.4		
Sr $3d_{3/2}$	135.8	135.5	SrO	(Ref 12-13)
Sr $3d_{5/2}$	134.06	133.5		
Al 2p	73.03	74.50	Al_2O_3	(Ref 14-17)
O 1s	528.19	528.73	Al_2O_3	(Ref 15)
O 1s	529.50	530.40	Sm_2O_3	(Ref 11)
O1s	530.10	530.20	SrO	(Ref 13)

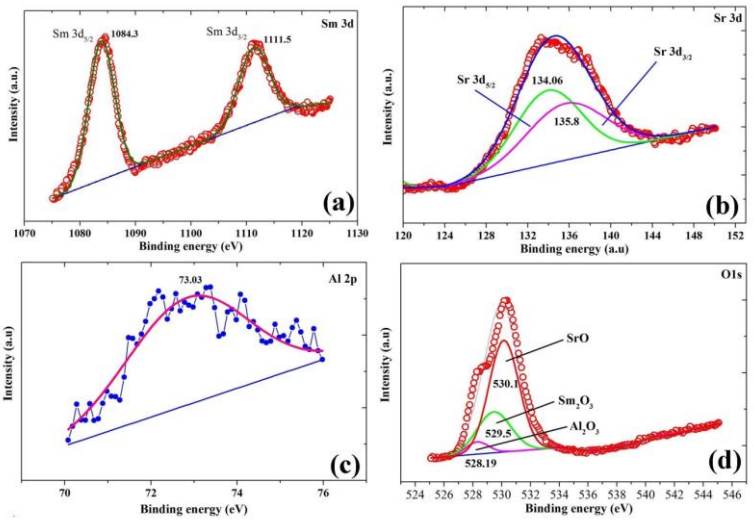

Fig. 2: Deconvoluted high resolution spectra of SSA ceramic powder: (a) Sm 3d; (b) Sr 3d; (c) Al 2p; and (d) O 1s.

3.2 Surface morphology of as synthesized SSA ceramic

Fig. 3 shows the surface morphology of as synthesized SSA ceramic and respective EDS analysis. The observed surface morphology of SSA particle was found to be cuboidal in shape (Fig. 3). In general cuboidal shape of particles would be observed in molten salt synthesis due to the mechanism of crystal growth in the chloride salts [18]. The elemental analysis of selected regions in Fig. 3 was done to find out the chemical composition of as synthesized SSA ceramic. The elemental compositions (at.%) of Sm, Sr, Al, and O were found to be 18.54, 8.08, 16.79 and 56.59 which is very similar to the theoretical stoichiometry of $Sm_2SrAl_2O_7$ (2:1:2:7) ceramic. So based on the XPS and EDS results confirm that the synthesized products correspond to single phase SSA without any impurities.

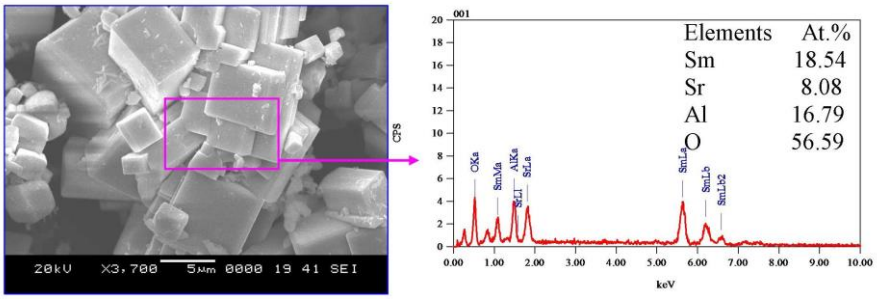

Fig. 3: Surface morphology of as synthesized SSA ceramic powder

3.3 Cross sectional micrograph of SSA after coatings

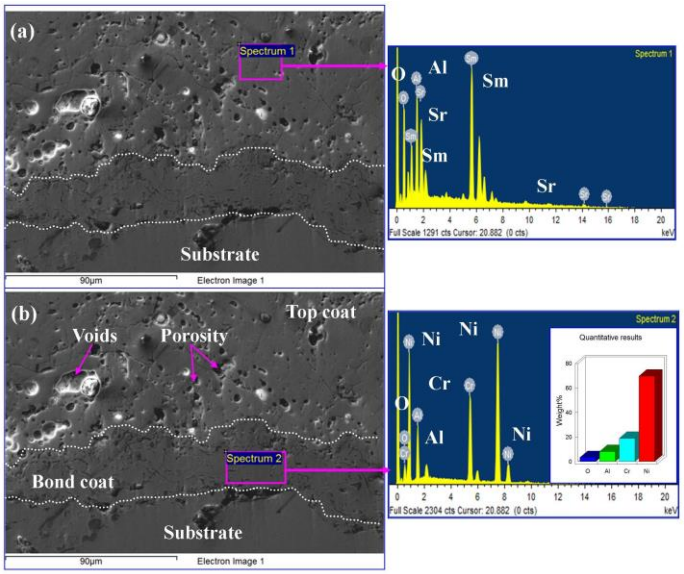

Fig. 4: (a and b) Cross sectional SEM microstructure of as deposited SSA TBCs. EDS analysis of region 1 in top coat (a); and region 2 in bond coat are also shown here.

Fig. 4 shows the cross sectional SEM micrographs and respective EDS analysis in the top coat (4a) and bond coat (4b) of as deposited SSA TBCs. The presence of voids and heterogeneous distributions of porosities were clearly seen in the Fig. 4 probably due to the presence of dissolved gases in the ceramic powder. The presence of such porosities and voids in the ceramic top coat TBC layer play a vital role in thermal shock resistance at higher temperature [19]. As compared to ceramic TBC (~1950 ºC) layer the metallic bond coat seems to be dense due to completing melting of NiCrAlY (~1400 ºC) particle in the plasma plume. The EDS analysis was conducted in the different places of as deposited coatings to know the chemical composition after plasma spraying process. The elemental analysis of selected region in Fig. 4 (a) shows the presence of Sm, Sr, Al and O (at.%) as 18.09, 7.95, 15.01 and 58.95 respectively. The obtained atomic percentage of Sm, Sr, Al and O which are similar to as synthesized SSA ceramic indicated that there is no compositional and any additional product formation during the plasma spraying process. The EDS analysis of selected region in the metallic bond coat shows the presence of Ni, Cr,

Al and O (69.75 wt.% Ni, 18.89 wt.% Cr, 8.16 wt.% Al and 3.20 wt.% O). A small amount of oxygen was also found in the metallic bond coat layer due to the oxidation of NiCrAlY during the deposition process.

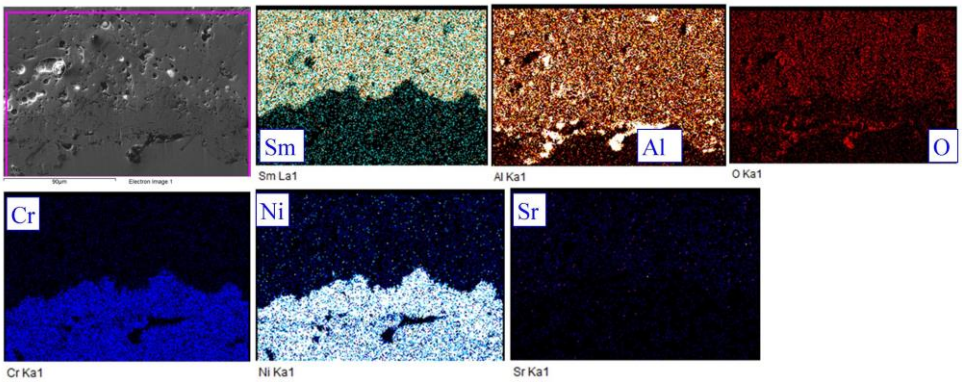

Fig. 5: Cross sectional EDS mapping analysis of as deposited SSA coatings

In order to understand the elemental interdiffusion between bond coat and top coat, the EDS elemental map scanning analysis was performed on the cross sectional sample. The map scanning images of Sm, Sr, Al, Ni, Cr, and O are shown in Fig. 5. It is observed that there is no interdiffusion of Sm from the top coat to bond coat and Ni or Cr from bond coat to ceramic top coat during the deposition process. Since the presence of Al in both top coat and bond coat, it is not able to distinguish the diffusion behavior by this analysis.

3.4 Mechanical properties of substrate, bond coat (NiCrAlY) and SSA TBCs

Fig. 6 shows the depth-time (6a) and load-depth (6b) curves of the substrate, metallic bond coat and as deposited SSA TBCs obtained from the polished sample surfaces (R_a<200 nm). The obtained mechanical properties such as stiffness, Young's modulus, and hardness are reported in Table 2. The load and depth variation of different layers of coatings were continuously measured during loading and unloading condition.

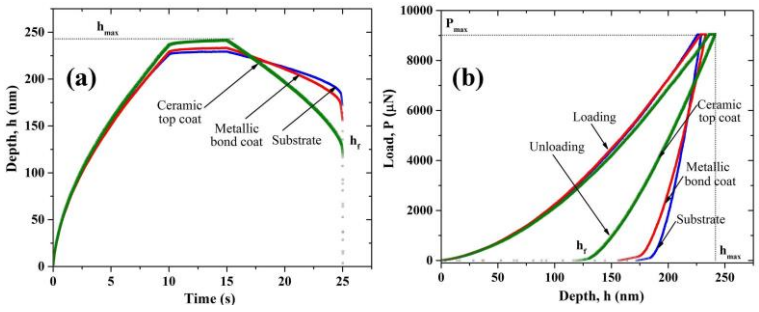

Fig. 6: Typical (a) depth-time; and (b) load-depth curves of substrate, metallic bond coat and as deposited SSA TBCs.

Table 2: Mechanical properties of substrate, metallic bond coat and as deposited SSA TBCs.

	Stiffness (μN/nm)	Young's modulus (GPa	Hardness (GPa)
Substrate	310±9	220±10	5.0±0.2
NiCrAlY bond coat	220±5	155±15	5.5±0.4
SSA TBC layer	110±3	80±0.3	6.1±0.5

The ceramic TBC showed maximum penetration depth of 267 nm followed by 235 nm for metallic bond coat and 223 nm for Inconel substrate material. The higher penetration depth observed for ceramic TBC layer may be due to the presence of defects such as micro pores and voids. The presence of such defects also decreased Young's modulus, hardness and stiffness of SSA TBC layer than the metallic bond coat and substrate material. The porosity of as deposited SSA TBCs was calculated to be about 65% using the theoretical relation between Young's modulus of solid and porous SSA ceramic. The load-depth curve of SSA TBCs also showed the highest elastic recovery of 49%, whereas for metallic NiCrAlY was about 25% and for Inconel substrate 19%. The highest elastic recovery of SSA TBCs was found due to the presence of higher porosity which can easily distribute the strain energy during loading and unloading condition. The lowest elastic recovery was obtained for the substrate which is due to dense nature; hence the maximum part of applied indentation load was utilized for the plastic deformation.

4 Conclusions

In the present study, the rare earth based samarium strontium aluminate ceramic was synthesized and coated on bond coated Inconel 718 substrate by air plasma spray process. There are no compositional changes of SSA ceramic was observed after the deposition process. The EDS mapping results showed that a negligible elemental interdiffusion between bond coat and top coat. The Young's modulus and hardness of SSA TBCs were found to be about 80 GPa and 6.1 GPa respectively. The highest elastic recovery was obtained for SSA ceramic top coat layer (49%) as compared to metallic bond coat (25%) and Inconel substrate (19%).

Acknowledgement

One of the authors (T. Baskaran) would like to thank the MHRD, Government of India, for a research scholarship. The authors acknowledge M/s. Metallizing Equipment Co. Pvt. Ltd, Jodhpur, India for providing plasma spray facility. The authors also thank Prof. U. Ramamurty (IISc, Bangalore) for providing the Nano-indentation facility.

References

1. R.A. Miller, Surf. Coat. Technol. **30**, 1-11, (1987).

2. G. Bertrand, P. Bertrand, P. Roy, C. Rio, and R. Mevrel, Surf. Coat. Technol. **202**, 1994-2001, (2008).

3. G. Moskal, L. Swadźba, M. Hetmańczyk, B. Witala, B. Mendala, J. Mendala, and P. Sosnowy, J. Eur. Ceram. Soc. **32**, 2035-2042, (2012).

4. H. Dong, Y. Ren, D. Wang, X. Li, Y. Bai, J. Wang, and W. Ma, J. Eur. Ceram. Soc. **34**, pp. 3917-3924, (2014).

5. W. Ma, S.K. Gong, H.B. Xu, and X.Q. Cao, Scripta Mater. **54**, 1505–1508, (2006).

6. C. Wan, T. D. Sparks, W. Pan, and D. R. Clarke, J. Amer. Ceram. Soc., **93**, 1457-1460, (2010).

7. J. Feng, B. Xiao, R. Zhou, W. Pan, and D. R. Clarke, Acta Mater. **60**, 3380-3392, (2012).

8. D.L. Hecht, K. Rohrmann, T. Stocker, and W. Thiel, Surf. Interface Anal. **39**, 845-851, (2007).

9. D. Petrov, B. Angelov, and V. Lovchinov, J. Rare Earths, **28**, 603-605, (2010).

10. Y. Uwamino, Y. Ishizuka, and H. Yamatera, J. Electron. Spectrosc. Relat. Phenom. **34**, 67-78, (1984).

11. C. D. Wagner, W.M. Riggs, L.E. Davis, J.F. Moulder, and G.E. Mullenberg, *Handbook of X-ray photoelectron spectroscopy*, Minnesota, (1979).

12. R. P. Vasquez, J. Electron. Spectrosc. Relat. Phenom. **56**, 217-240, (1991).

13. T. X. Wang, and W.W. Chen, Mater. Lett. **62**, 2865-2867, (2008).

14. B. R. Strohmeier, Surf. Sci. Spectra, **3**, 141-146, (1994).

15. N. Reddy, P. Bera, V.R. Reddy, N. Sridhara, A. Dey, C. Anandan, and A.K. Sharma, Ceram. Int. **40**, 11099-11107, (2014).

16. N.H. Turner, and A.M. Single, **15**, 215-222, (1990).

17. E. Gillet, and B. Ealet, Surf. Sci. **273**, 427-436, (1992).

18. C. Mao, G. Wang, X. Dong, Z. Zhou, and Y. Zhang, Mat. Chem. Phy. **106**, 164-167, (2007).

19. H. Guo, S. Kuroda, and H. Murakami, J. Am. Ceram. Technol. **89**, 1432-1439, (2006).